RESEARCH PAPER

Acta Neurobiol Exp 2020, 80: 139–159
DOI: 10.21307/ane-2020-014

since 1928 ACTA NEUROBIOLOGIÆ EXPERIMENTALIS

Dependence of the filled-space illusion on the size and location of contextual distractors

Vilius Marma[1,2], Aleksandr Bulatov[1,2] and Natalija Bulatova[2]

[1] Laboratory of Visual Neurophysiology, Lithuanian University of Health Sciences, Kaunas, Lithuania,
[2] Institute of Biological Systems and Genetics Research, Lithuanian University of Health Sciences, Kaunas, Lithuania,
** Email: aleksandr.bulatov@lsmuni.lt*

For most observers, the part of the stimulus that is filled with some visual elements (e.g., distractors) appears larger than the unfilled part of the same size. This illusion of interrupted spatial extent is also known as the 'filled-space' or 'Oppel-Kundt' illusion. Although the continuously filled-space illusion has been systematically studied for over a century, there is still no generally accepted explanation of its origin. The present study aimed to further develop our computational model of the continuously filled-space illusion and to examine whether the model predictions successfully account for illusory effects caused by distracting line-segments of various lengths that are attached to different endpoints (i.e., terminators) of the reference spatial interval of the three-dot stimulus. Our experiments confirm that the illusion manifests itself along a distracting segment located both inside and outside of the reference interval. In the case of two distractors arranged symmetrically with respect to the lateral terminator, we found that the magnitude of the illusion is approximately equal to the sum of the relevant values obtained with separate distractors. The results of experiments using vertical shifts of distractors supported the model's assumption regarding the two-dimensional Gaussian profile of hypothetical areas of weighted spatial summation of neural activity. A good correspondence between the experimental and theoretical results supports the suggestion that perceptual positional biases associated with the context-evoked increase in neural excitation may be one of the main causes of the continuously filled-space illusion.

Key words: length misjudgment, filled-space illusion, spatial summation, Oppel-Kundt figures

INTRODUCTION

In the illusion of interrupted spatial extent and modifications thereof (i.e., the filled-space or Oppel-Kundt illusion), the part of the stimulus that is filled with some visual elements appears larger than the unfilled part of the same size. The illusion of interrupted spatial extent remains one of the least understood among the many visual-geometric illusions of spatial extent. In other words, there is still no general consensus regarding the origin or the definition of the illusion. This is a significant gap given that numerous studies have attributed a wide range of characteristics to this phenomenon (cf. Wackermann, 2017). For example, several studies have reported a sharp increase in the magnitude of the length-matching errors that increases to a certain value of the number of evenly distributed identical fillers (Obonai, 1933; Spiegel, 1937; Piaget and Osterrieth, 1953; Coren et al., 1976; Noguchi et al., 1990; Bulatov et al., 1997; Wackermann and Kastner, 2010). This is known as the conventional Oppel-Kundt stimulus (Fig. 1A). The Oppel-Kundt illusion occurs while viewing not only simple flat drawings, but also in viewing complex three-dimensional stimuli (Deregowski and McGeorge, 2006). In experiments with two-dimensional patterns filled with various textures, it was demonstrated that manipulations with the spatial frequency of the filling significantly affect the perceived size of the textured area (Giora and Gori, 2010). The illusion survives – albeit in a somewhat weakened form – with an irregular (Lewis, 1912; Noguchi, 2003;

Received 7 June 2019, accepted 11 February 2020

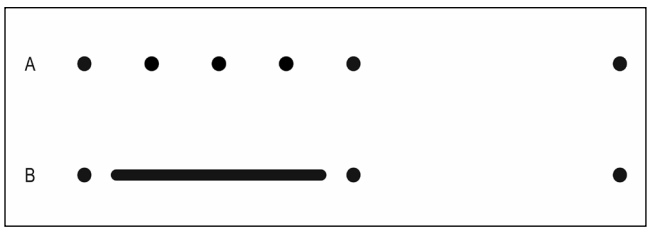

Fig. 1. Examples of different figures that induce geometric illusions of interrupted spatial extent. (A) The conventional Oppel-Kundt figure with equally spaced distracting dots (i.e., discrete fillers). (B) The three-dot figure with a distracting line-segment (i.e., continuous filler).

Wackermann and Kastner, 2009) or high-density filling (Bailes, 1995; Bertulis and Bulatov, 2001). The magnitude of the illusion increases slightly with an increase in the figure/background luminance contrast (Long and Murtagh, 1984; Dworkin and Bross, 1998; Wackermann, 2012), but decreases with an increase in the absolute luminance or color contrast between the stimuli elements (Bulatov and Bertulis, 2005; Surkys, 2007).

The Oppel-Kundt illusion depends not only on spatial and luminance parameters of the stimulus, but also varies significantly with changes in the temporal duration (Bailes, 1995; Dworkin and Bross, 1998) and the method of stimuli observation. An increase in stimulus duration in the range of about 100 to 1000 ms leads to a gradual strengthening of the Oppel-Kundt illusion until saturation occurs. This time-dependent effect suggests the involvement of some time-consuming integration processes in the development of the full-scale illusion (Bertulis et al., 2014). Voluntary saccades when observing a stimulus have been shown to significantly weaken the illusion (Coren and Hoenig, 1972). Other research shows that fixation of the gaze in the filled part of the stimulus causes a much stronger illusory effect than fixation in an empty spatial interval (Piaget and Bang, 1961).

There are currently few known explanations of the Oppel-Kundt illusion. Moreover, most of the explanations are inherently qualitative and thus, are unable to make predictions that can be unambiguously verified in experiments. The existing explanations are also limited in that, as a rule, they concern only a subset of features of a given stimulus that contain the discrete periodical filling. For instance, according to a proposed explanation reported by Taylor (1962), the occurrence of the Oppel-Kundt illusion is related to perceptual spatial separation of contextual fillers. To some extent, Taylor's explanation resonates with an idea set forth by Craven and Watt (1989) and Watt (1990), who suggested that the number of zero-crossings of the spatial profile of neural excitation largely determines the strength of the illusion. These explanations are supported by experimental evidence for the relevance of clear discriminability of lines filling some rectangular shape (Botti, 1906) or microelements of textured patterns (Giora and Gori, 2010). However, it is clear that these explanations can only be applied to account for data collected with stimuli that are comprised of clearly articulated and discrete filling. In this respect, the explanation proposed by Bertulis et al. (2014) may be more suitable because it does not have these apparent limitations regarding the filling structure. According to this approach, the emergence of an illusion can be associated with the processes of spatial-temporal integration along the continuous path of overlapping patterns of cortical neural activation (Field et al., 1993; Kojo et al., 1993; Hirsch et al., 1995). Unfortunately, the theory proposed by Bertulis et al. (2014) is still purely qualitative.

The effects of different modification (e.g., spatial convolution, integration, or differentiation) of activation profiles are employed in the Oppel-Kundt illusion explanation concerned with spatial-frequency filtering. Importantly, spatial-frequency filtering is an inherent feature of neural processing starting from the lowest levels of the visual system (e.g., receptive fields of retinal ganglion cells). According to this approach (Ganz, 1966; Bulatov et al., 1997; Surkys, 2007), the spatial-frequency filtering performed by receptive fields of neurons in different cortical areas (i.e., V1 and higher) results in positional biases of specific loci in the profile of neural excitation, thereby inducing distortions in the perception of length. Although some investigators have previously claimed that effects related to filtering are likely too small to account for an actual magnitude of length misjudgment (Rentschler et al., 1975; Mikellidou and Thompson, 2014), filtering-induced distortions remain among the most widely accepted explanations for the Oppel-Kundt illusion. However, it should be recognized that, to-date, there are no well-established theories of this perceptual phenomenon. Therefore, other quantitative methods for explaining this illusion should be mentioned. These quantitative methods use analogies with physical force fields (Eriksson, 1970) or mathematical methods of information processing (Erdfelder and Faul, 1994), but lack a strong neurophysiological basis. A purely phenomenological approach uses a straightforward constructing of functions that are most suitable for fitting experimental data (Wackermann and Kastner, 2010).

It is noteworthy that most studies of the Oppel-Kundt illusion have focused on effects related to the periodicity (or spatial frequency) of discrete filling of stimuli. These studies have largely ignored the fact that, although the illusion systematically weakens with increasing filling density, it remains quite significant when tightly packed individual fillers actually merge

into a single continuous entity (Bailes, 1995; Bulatov et al., 1997; Wackermann and Kastner, 2010). A specific feature of our current study is that it addresses issues related to this particular modification of the illusion. Recently, we performed psychophysical experiments with stimuli that contain a continuous distractor (Fig. 1B). We demonstrated that length misjudgments are primarily associated with the integration of distractor-evoked effects in regions near the endpoints (i.e., terminators) of stimulus spatial intervals (Bulatov et al., 2017). In addition, we proposed a preliminary quantitative interpretation of the experimental results. However, it should be emphasized that, although the proposed model is quite suitable for reproducing one of the most widely-known features of the Oppel-Kundt illusion (i.e., the non-monotonic dependence of the illusion on the number of discrete fillers), we currently cannot directly identify effects caused by continuously filled stimuli with effects evoked by the conventional Oppel-Kundt figures. Therefore, in order to avoid confusion with historically established definitions, we use in our study a more neutral name – the continuously filled-space illusion (cFSI) – for the visual phenomenon under consideration. Contrary to the view that the illusion may arise due to changes in the shape of the excitation profile (or positional distortions caused by spatial filtering), the model of the cFSI is concerned with a context-induced increase in the overall neural response of some hypothetical subsystem of encoding of retinal coordinates of stimulus terminators. The subsequent improvement of the model provided some additional predictions regarding the illusion manifestation and allowed for the relatively successful interpretation of new experimental data obtained with the most elementary stimulus comprising a single-dot distractor (Bulatov et al., 2019). Thus, even in its highly simplified and unfinished form, the model gave a unified explanation of the experimental results accumulated for stimuli that differ significantly in spatial structure. Given that, at present, there are no other successful (and quantitative) theories of the illusion, we propose that a comprehensive experimental study of the illusory effects for the widest possible range of stimulus modifications is needed. We also propose that a careful theoretical analysis and justification of the principles underlying the model calculations will together provide a potentially fruitful road map for future research. We believe that a quantitative computational approach offers a sufficiently rigorous description of the behavior of the illusion under different variations of stimulus parameters, for example, by explicitly specifying the properties of the curves of functional dependencies. We contend that this approach also provides an immediate and purposeful experimental verification of the model predictions with a simultaneous check of the model's falsifiability.

In the present study, we continue to examine the proposed cFSI model by assessing the adequacy of its predictions (i.e., pre-calculated functional dependencies) regarding illusory effects evoked by previously untested stimuli that contain contextual line-segments of various sizes and locations. Since the basic computational principles of the model have been developed for the most elementary stimulus made up of few separate dots (Bulatov et al., 2019), we expected that the success (or failure) in applying model calculations to predict the illusory effects caused by stimuli that contain line distractors would provide a significant advance in our understanding of the phenomenon under study. That is, the acquired data would at least demonstrate the applicability of spatial integration procedures that can be used to explain the illusion. To verify the predictions, we performed four series of psychophysical experiments in order to quantitatively determine the magnitude of the illusion as a function of the length (d) of distracting line-segments attached to different terminators (t_R, t_C, and t_T) of the reference spatial interval of the three-dot stimulus (Fig. 2A-D). According to the model, the illusion is determined by the integration of distractor-induced additional excitation in the regions surrounding the stimulus terminators. Next, we tested the validity of the model, specifically the assumptions regarding the shape and parameters of the two-dimensional weighting function of these putative areas of summation of neural activity. To this end, we conducted a fifth series of experiments with the distractor's position shifted (h) in the direction that is orthogonal to the stimulus axis (Fig. 2E). The use of stimuli with a minimal set of simple homogeneous elements (i.e., line-segments) made it possible to largely eliminate poorly identifiable irrelevant parameters. This stimulus set also facilitated the theoretical analysis of the experimental results.

In our previous studies on the cFSI (Bulatov et al., 2017; 2019), we proposed a rather simple interpretation of the experimental results that was based on the assumption that length judgments are associated with neural calculations of retinal coordinates of stimulus terminators. We previously suggested that information about the terminator's coordinates is encoded by the magnitude of the response of some hypothetical area of weighted spatial integration (or attentional window of summation, AWS) centered at the terminator. In this regard, we also proposed that the input neural excitation (to AWS) should be normalized to a certain constant range (e.g., between 0 and 1), which is necessary to ensure amplitude-independent conditions for unambiguous encoding of the coordinates. In

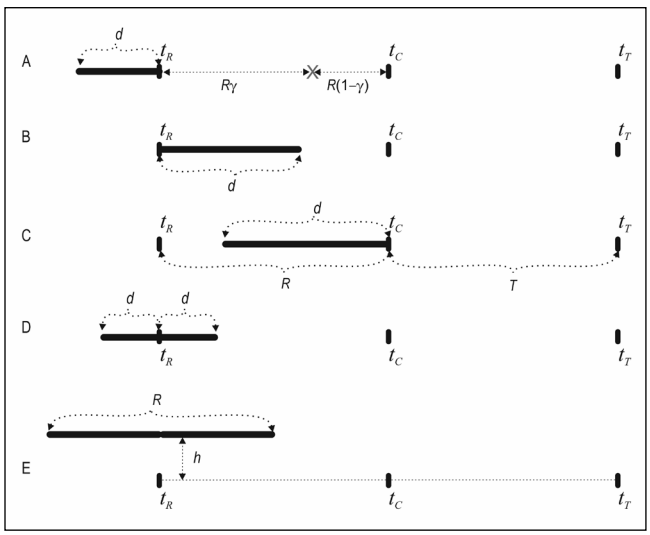

Fig. 2. Examples of stimuli used in experiments. The three-dot stimuli are comprised of short vertical ticks t_R, t_C, and t_T. These vertical ticks serve as distracting line-segments that are placed either outside (A) or inside (B and C) of the reference interval. The stimuli are comprised of two symmetrically arranged (relative to the terminator t_R) segments presented on the stimulus axis (D) or shifted vertically (E). *R* and *T*, the length of the reference and test interval, respectively; *d*, the length of the distractor; *h*, the vertical offset of distractors; γ, the coefficient determining the position of gaze fixation X. See text for additional information. *Dotted lines*, the dimensions were not part of the actual display. In experiments, white stimuli (luminance of all the ticks and lines, 20 cd/m^2) were presented against a dark round-shaped background (8° in diameter and 0.4 cd/m^2 in luminance).

other words, we assumed that the greater distance between the fovea and the terminator (i.e., its eccentricity) is associated with a wider aggregated profile of overlapping receptive fields affected by this terminator, thus inducing a larger integrated response of the corresponding AWS (and *vice versa*, greater response is related to perceptually larger eccentricity of a target). The above suggestions are indirectly supported by human fMRI data (Dumoulin and Wandell, 2008; Silva et al., 2018; Welbourne et al., 2018) on eccentricity-dependent changes in the size of the neuronal population receptive field (pRF) and the results of extracellular recordings from the lateral intraparietal area (LIP) of macaque monkeys (Sereno and Lehky, 2011; Graf and Andersen, 2014; Bremmer et al., 2016). Indeed, these prior studies demonstrate that the size of the pRF linearly increases with increasing eccentricity, and that changes in activity of the LIP population allow quite reliable predictions of the target distance, as well as, the size of an upcoming saccade and its direction. In turn, the use of a normalization procedure agrees with numerous reports in the literature (Reynolds and Heeger, 2009; Olsen et al., 2010; Carandini and Heeger, 2012; Vokoun et al., 2014) showing that normalization plays an important role in neural information processing.

Here, we will briefly introduce the model's principal computational procedure developed by Bulatov et al. (2019) for an elementary stimulus made up of two separate dots (i.e., a terminator and a distractor). Then, we apply this procedure in calculations of illusory effects for stimuli that are comprised of contextual line-segments. Assuming, for simplicity, the same size for the circular Gaussian profiles (whose dimensions scale linearly with retinal eccentricity) of neural excitation (*I*) and AWS (*A*), the magnitude (*S*) of the response evoked by a single dot (e.g., stimulus terminator) presented at eccentricity (ρ) can be evaluated by the integration of the product of two Gaussians (Bulatov et al., 2019):

$$S(\rho)=\iint_{\infty} A(x,y,\rho)I(x,y,\rho)dxdy=\iint_{\infty} e^{-\frac{x^2+y^2}{\left(k|\rho|+\sigma_0\right)^2}}dxdy=\pi\left(k|\rho|+\sigma_0\right)^2=\pi\sigma(\rho)^2, \quad (1)$$

where k and σ_0 represent the slope and the intercept of the linear regression of the standard deviation σ(ρ), respectively.

In turn, the appearance of a contextual distractor near the stimulus terminator should increase the cumulative response of relevant AWS, which is due to the distractor-evoked additional excitation s_{add}. Then, given the assumption that this response augmentation can be interpreted by the visual system as a bias (δ) in perceived localization of the terminator, $S(\rho+\delta)=S(\rho)+s_{add}$, the value of the bias can be determined from Formula 1 as follows (Bulatov et al., 2019):

$$\delta=\mathrm{sgn}(\rho)\frac{\sqrt{S(\rho)+s_{add}}-\sqrt{S(\rho)}}{k\sqrt{\pi}}, \text{ and, when } s_{add} \ll S(\rho), \delta\approx\frac{\mathrm{sgn}(\rho)s_{add}}{2k\pi\sigma(\rho)} \quad (2)$$

where *sgn*(.) represents the *sign* function.

The proposed principle of calculations can be extended to stimuli with distractors of different spatial structure and location. Moreover, because of the symmetry of spatial profile of the terminator-related AWS, it immediately follows that the perceptual positional biases should emerge approximately equally for stimuli with distractors located either inside (Fig. 2B) or outside (Fig. 2A) of the reference interval. Besides, due to nearly linear dependence of the bias δ on the value of additional excitation s_{add}, the illusory effects should be about twice as strong in the case of two distractors arranged symmetrically with respect to the lateral terminator (Fig. 2D).

The magnitude of the illusory displacement of stimulus terminator depends on the size of the corresponding AWS, which linearly increases with retinal eccentricity. That is, the magnitude depends on the actual position of gaze fixation. To account for the effects of eccentricity, we use a certain coefficient (γ), and, for simplicity, consider only the fixation points located on the horizontal *x*-axis of the stimulus (i.e., 0≤γ≤2). For example, a coefficient value between 0 and 1 indicates that the gaze is fixated (Fig. 2A, the position $R\gamma$ relative to the lateral terminator t_R) within the reference stimulus interval. For the values between 1 and 2, in contrast, the fixation is shifted to the test interval.

As an example, we can take the general case of stimuli with two distractors, e.g., two line-segments of the length (*l*) and (*r*) located on the left and right relative to the lateral stimulus terminator, respectively. For these stimuli, the two-dimensional spatial profile of additional excitation can be described by the positive part of the function that represents the difference between the profiles of stimulus-evoked excitation in the presence and absence of the distractors:

$$F(x,y,l,r,h,\sigma_\gamma)=\left(M(x,y,l,r,h,\sigma_\gamma)-e^{-\frac{x^2+y^2}{2\sigma_\gamma^2}}\right)e^{-\frac{x^2+y^2}{2\sigma_\gamma^2}}\approx\left[\left(H(x+l)-H(x-r)\right)e^{-\frac{(y-h)^2}{2\sigma_\gamma^2}}-e^{-\frac{x^2+y^2}{2\sigma_\gamma^2}}\right]e^{-\frac{x^2+y^2}{2\sigma_\gamma^2}}, \quad (3)$$

where $\sigma_\gamma=kR/|\gamma|+\sigma_0$ is the standard deviation of the Gaussian function of the AWS centered at the lateral terminator t_R; *h* is the vertical offset of distractors; $M(x,y,l,r,h,\sigma_\gamma)$ represents the normalized two-dimensional spatial profile of neural excitation caused by the distractors. Bearing in mind the effect of strong attenuation towards the periphery the Gaussian profile of the AWS, for the sake of simplicity, we can reasonably approximate (Fig. 3) the profile of the distractor-evoked excitation along the stimulus *x*-axis as a piecewise-constant function. That is, we can use the difference of the two Heaviside step functions *H*(.) instead of a more complex function *M*(.). In turn, the positive part of Function 3 can be obtained by using, once again, the Heaviside step function in the following formula:

$$P(x,y,l,r,h,\sigma_\gamma)=F(x,y,l,r,h,\sigma_\gamma)H\left(F(x,y,l,r,h,\sigma_\gamma)\right), \quad (4)$$

With an appropriate choice of the parameters in Formula 3, the cumulative response of the "lateral" AWS (i.e., the AWS centered on the lateral terminator t_R) for the stimulus shown in Fig. 2A (i.e., stimulus that is comprised of a single external distracting line-segment) can be described with a rather simple analytical expression:

$$QL_{out}(d,\sigma_\gamma)=S(R\gamma)+\int_{-\infty}^{\infty}\left(\int_{-d}^{0}P(x,y,d,0,0,\sigma_\gamma)dx\right)dy=\frac{\pi\sigma_\gamma^{\,2}}{2}\left[2+\sqrt{2}erf\left(\frac{d}{\sqrt{2}\sigma_\gamma}\right)-erf\left(\frac{d}{\sigma_\gamma}\right)\right], \quad (5)$$

where *R* and *d* represent the length of the reference stimulus interval and the length of distractor, respectively; *erf*(.) is the error function encountered for the integration of a normalized Gaussian function.

Due to the symmetry of the profile of AWS, we can expect the same dependence of the magnitude of the cumulative response on the length of the distracting line-segment located inside the reference interval (Fig. 2B), i.e., $QL_{ins}(d,\sigma_\gamma)=QL_{out}(d,\sigma_\gamma)$. Accordingly, in the case of two distractors arranged on the stimulus *x*-axis symmetrically relative to the lateral terminator (Fig. 2D), the magnitude of the relevant cumulative response can be described as $QL_{sym}(d,\sigma_\gamma)= 2QL_{out}(d,\sigma_\gamma) - S(R\gamma)$. Next, if we change the length parameters for

relevant distractors and also change the corresponding limits of integration along the *x*-axis in Formula 5, the cumulative response of the "lateral" AWS can be calculated in a similar manner for a stimulus (Fig. 2C) with distracting line-segment attached to the central terminator t_C:

$$QL_{cnt}(d,\sigma_\gamma)=\frac{\pi\sigma_\gamma^{\,2}}{2}\left[2+\sqrt{2}\left[erf\left(\frac{R}{\sqrt{2}\sigma_\gamma}\right)-erf\left(\frac{R-d}{\sqrt{2}\sigma_\gamma}\right)\right]-\left[erf\left(\frac{R}{\sigma_\gamma}\right)-erf\left(\frac{R-d}{\sigma_\gamma}\right)\right]\right], \quad (6)$$

Using Formulas 3 and 4 for stimuli with vertically shifted distractors (Fig. 2E), whenever the vertical offset (h) is not equal to zero, the magnitude of the cumulative response (QL_{off}) of the "lateral" AWS can be calculated as follows:

$$QL_{off}(h,\sigma_\gamma)=S(R\gamma)+\frac{\sqrt{\pi}\sigma_\gamma}{2}\int_{-0.5R}^{0.5R}\left[e^{-\frac{(2x^2+h^2)}{4\sigma_\gamma^{\,2}}}\left(1+erf\left(\frac{x^2}{2|h|\sigma_\gamma}\right)\right)-e^{-\frac{x^2}{\sigma_\gamma^{\,2}}}\left(1+erf\left(\frac{x^2-h^2}{2|h|\sigma_\gamma}\right)\right)\right]dx, \quad (7)$$

In the case of the vertical offset equal to zero, Equation 7 reduces to that for the stimulus shown in Fig. 2D, therefore the expression $QL_{off}(0,\sigma_\gamma)=QL_{sym}(0.5R,\sigma_\gamma)$ can be used.

In turn, the presence of the distractor within the reference interval should also increase the cumulative response (QC) of the "central" AWS (i.e., the AWS centered on the stimulus terminator t_C). To evaluate this response, Formulas 5 – 7 can again be used after the corresponding change of the integration limits and after taking into account the window location with respect to the gaze fixation point (i.e., by substituting $\sigma_\gamma=kR|\gamma|+\sigma_0$ with $\sigma_{1-\gamma}=kR|1-\gamma|+\sigma_0$). For example, in the case of the stimulus (Fig. 2B) with the distracting line-segment attached to the terminator t_R, the magnitude of the response can be evaluated using Formula 6, i.e., $QC_{lat}(d,\sigma_{1-\gamma})=QL_{cnt}(d,\sigma_{1-\gamma})$. Similarly, we can use the same formula for the stimulus shown in Fig. 2D because the external distractor has only a negligible effect. Similarly, the window response in the case (Fig. 2C) of distractor attached to the terminator t_C can be assessed by Formula 5, i.e., $QC_{cnt}(d,\sigma_{1-\gamma})=QL_{out}(d,\sigma_{1-\gamma})$.

According to Formula 2, an increase in the response (QL) of the "lateral" AWS should cause a perceptual change in the corresponding terminator coordinate (X_R) along the stimulus *x*-axis:

$$X_R=-\mathrm{sgn}(\gamma)\delta_R=-\mathrm{sgn}(\gamma)\frac{\sqrt{QL(d,\sigma_\gamma)}-\sqrt{S(R\gamma)}}{k\sqrt{\pi}}, \quad (8)$$

where the sign before the bias δ_R depends on the gaze fixation position. This position is negative, for con-

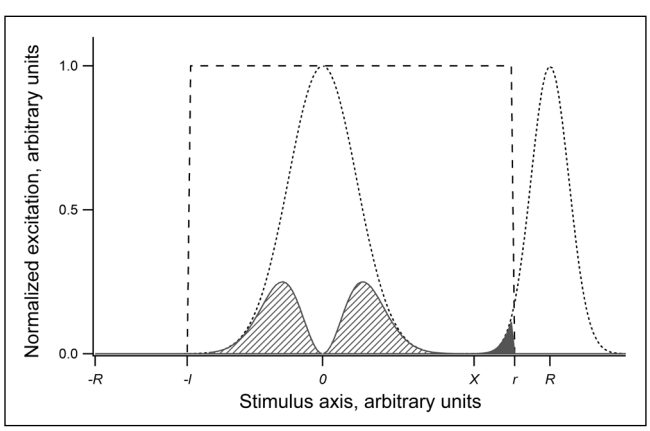

Fig. 3. Diagrams illustrating the model calculations. The dotted curve represents the normalized profile of excitation caused by the lateral (located at 0) and central (located at R) stimulus terminators. Dashed line, the schematic representation of the normalized profile of excitation caused by two distracting line-segments located on the left (the length *l*) and right (the length *r*) relative to the lateral stimulus terminator. Of note, the vertical offset of distractors is equal to zero; X represents the position of gaze fixation. The areas indicated by the hatched and filled regions represent the additional excitation related to the lateral and the central AWSs, respectively.

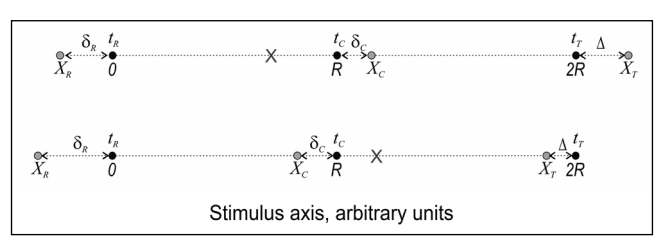

Fig. 4. Diagrams illustrating the calculations of the illusion magnitude Δ using Formula 10. δ_R and δ_C represent the perceptual positional biases of terminators t_R (located at 0) and t_C (located at *R*), respectively; X_R, X_C, and X_T represent the perceived coordinates of corresponding terminators. The sign of the bias δ_C depends on the gaze fixation position X. δ_C is positive when the gaze is directed to the reference stimulus interval (i.e., upper row), and is negative for fixations within the test interval (i.e., lower row).

ditions wherein the gaze is directed to the right relative to the terminator t_R and positive for all other conditions. An increase in the cumulative response (QC) of the "central" AWS is likely accompanied by a perceptual change in the central terminator coordinate (X_C):

$$X_C = R + \mathrm{sgn}(1-\gamma)\delta_C = R + \mathrm{sgn}(1-\gamma)\frac{\sqrt{QC(d,\sigma_{1-\gamma})} - \sqrt{S(R(1-\gamma))}}{k\sqrt{\pi}}, \tag{9}$$

where the sign before the bias δ_C is positive in the case of the gaze directed to the left with respect to the terminator t_C.

In experiments, the task of the subjects is to move the lateral terminator t_T of the test interval into a position $X_T=2R+\Delta$, that makes both stimulus parts perceptually equal in length (Fig. 4). Therefore, the perceived coordinate X_C can be considered as the arithmetic mean of the coordinates X_R and X_T. Then, for the gaze fixated somewhere within the reference or test stimulus interval, the magnitude of the illusion (Δ) can be obtained from the following equation:

$$\Delta = \delta_R + 2sgn(1-\gamma)\delta_C, \tag{10}$$

Here, for the sake of simplicity, we considered only the idealized way of viewing the stimulus with a single gaze fixation point. However, real observations take place without any restrictions regarding the eye movements and distribution of attention. Thus, the illusion magnitude may strongly depend on the individual pattern of gaze fixations during perceptual evaluation of stimulus spatial parameters (Krauzlis et al., 2017). In order to roughly estimate account for the uncertainty related to individual differences in stimuli viewing, we can consider some particularly extreme cases. For example, when the subject holds the gaze fixated within one of the stimulus intervals (either reference or test), the bias δ_C, according to Formula 10, makes a double contribution (with a corresponding sign) to the resulting illusion magnitude. On the other hand, some two-phase sequential procedure of stimulus observation can be suggested. In particular, to assess and compare interval lengths, the subjects alternately and roughly symmetrically allocate their gaze between these intervals. Then the central terminator biases for these different gaze allocations are of opposite signs and largely compensate for each other; thus, their joint effect on the illusion magnitude should be close to zero. Therefore, if we assume some averaged combination of different ways of viewing the stimulus, it seems reasonable to use a certain coefficient (β, which value ranges between -1 and 1) in Formula 10 rather than a discontinuous *sign* function. In this case, the magnitude of the illusion can be described using the following equation:

$$\Delta(d,k,\gamma,\beta) = \frac{\sqrt{QL\left(d,\sigma_\gamma\right)} - \sqrt{S\left(R\gamma\right)}}{k\sqrt{\pi}} + 2\beta\frac{\sqrt{QC\left(d,\sigma_{1-\gamma}\right)} - \sqrt{S\left(R(1-\gamma)\right)}}{k\sqrt{\pi}}, \tag{11}$$

where d represents the length (or the vertical offset, in the case of the stimulus shown in Fig. 2E) of the distracting line-segment; QL and QC represent cumulative responses (calculated by relevant formulas) of the "lateral" and "central" AWS, respectively.

The model calculations predict a relatively simple shape of the curves for stimuli that are comprised of a single distracting line-segment positioned outside the reference interval (Fig. 5A) because only the contribution from the "lateral" AWS determines the effect of the cFSI. As can be seen from the graphs, the magnitude of the illusion gradually increases for relatively short distractors and saturates afterwards. Besides, the illusion significantly depends on the size of the relevant AWS (i.e., on the actual position of gaze fixation γ). The same holds true for stimuli with distractors attached to the lateral terminator from inside the reference interval (Fig. 5B); however, the magnitude of the illusion further increases (or reduces) with the distractor lengthening and approaching the central terminator. This exacerbating effect is due to the appearance of perceptual biases of the central terminator. Likewise, the dependence of the illusion on the gaze fixation position can be clearly seen (Fig. 5C) for stimuli with a single distracting line-segment attached to the central stimulus terminator. It is noteworthy that in this case, even a slight shift of the gaze towards the test interval leads to negative values of the illusion magnitude for an incompletely filled reference interval. However, the sign of the magnitude is inverted when

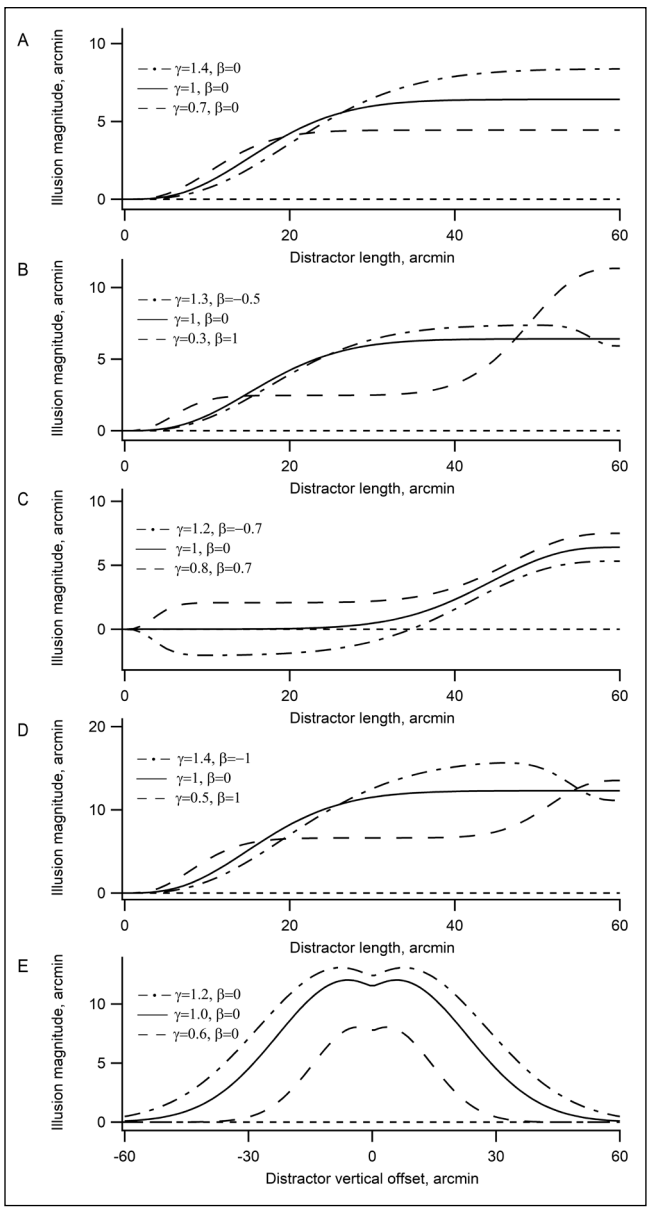

Fig. 5. The model predictions of the illusion magnitude. In rows (A) and (B) the stimuli used consisted of the distractor attached to the lateral terminator from outside and inside the reference interval, respectively. In row (C), the distractor was attached to the central terminator; in row (D), two distractors were arranged symmetrically relative to the lateral terminator; and in row (E), the distractors were shifted vertically. Legends show the values of the model parameters (γ and β). In calculations, we used values of slope k=0.2 and intercept σ_0=1 arcmin, which specify the linear dependence on eccentricity for the standard deviation of the Gaussian profile of AWS. The length of the reference interval R was equal to 60 arcmin.

the long distractor approaches the lateral terminator. Regarding the stimulus with two line-segments aligned symmetrically relative to the lateral terminator, the model predicts (Fig. 5D) that for the same viewing conditions, the illusion should be approximately twice as strong as in the case of stimuli with a single distractor. This is due to symmetrical spatial pooling of neural excitation within the terminator-related AWS.

Given the assumption concerning the two-dimensional properties of profiles of AWS and corresponding neural excitation, for stimuli with vertically shifted distractors (Fig. 2E), the model predicts the curves that are quite similar to Gaussian functions but with minor dips at their peaks (Fig. 5E).

Again, it should be emphasized that, since the values of perceptual biases caused by contextual distractors strongly depend on the retinal eccentricity of stimulus elements, the illusion magnitude may vary greatly and in a relatively complex manner with shifts in the actual direction of the observer's gaze. Therefore, the curves shown in Fig. 5 should be considered to be only as an illustration of some particular cases for arbitrarily chosen idealized conditions of stimuli observations. Nonetheless, on average, a certain correspondence between the model calculations and the values of the illusion magnitude, obtained from experiments, can be expected.

METHODS

Apparatus

All experiments were carried out in a dark room (the surrounding illumination<0.2 cd/m^2). A Sony SDM-HS95P 19-inch LCD monitor (spatial resolution 1280 × 1024 pixels, frame refresh rate 60 Hz) was used for stimuli presentations. A Cambridge Research Systems OptiCAL photometer was applied as a means of the monitor luminance range calibration and gamma correction. A chin and forehead rest was used to maintain a constant viewing distance of 200 cm (at this distance each pixel subtended about 0.5 arcmin); an artificial pupil (an aperture with a 3 mm diameter of a diaphragm placed in front of the eye) was applied to reduce optical aberrations.

Stimuli were presented in the center of a round-shaped background of about 8º in diameter and 0.4 cd/m^2 in luminance. Of note, the monitor screen was covered with a black mask with a circular aperture to prevent observers from being able to use the edges of the monitor as a vertical/horizontal reference. For all stimuli drawings, the Microsoft GDI+ antialiasing technique was applied to avoid jagged-edge effects.

Stimuli

The stimuli used in the experiments consisted of three horizontally distributed vertical ticks (lumi-

nance, 20 cd/m^2), which served as the terminators (t_R, t_C, and t_T, Fig. 2). These vertical ticks specified the ends of the reference and test stimulus intervals. The height and width of each tick were about 3 and 1 arcmin, respectively. The use of ticks instead of dots was necessary to ensure that the terminators were visible in the case of symmetrically attached distractors. Three different stimulus sizes were used in the study. The length (R) of the reference interval was fixed at 30, 60, and 90 arcmin.

In the experiments of the first four series, the length (d) of the distracting line-segment (line-width, 1 arcmin; luminance, 20 cd/m^2) was randomly changed in a range from 0 to R. In the first and the second series of experiments, a single line-segment (attached to the lateral terminator t_R) was placed outside (Fig. 2A) and inside (Fig. 2B) the reference interval, respectively. In the third series of experiments, a single distractor attached to the central stimulus terminator t_C was used (Fig. 2C). In the fourth series of experiments, two distracting line-segments were presented symmetrically on the stimulus axis, with respect to the lateral stimulus terminator (Fig. 2D). In the fifth series of experiments, the offset h of the line-segments (Fig. 2E) was randomly changed in a range from -R to R in the direction orthogonal to the stimulus axis (the length of each segment was fixed at $0.5R$).

Procedure

The method of adjustment was used in the study because, irrespective of its relative roughness and susceptibility to various cognitive biases, this method provides a reasonably simple and time-efficient way to collect enough data to ensure reliable fitting of the experimental curves with the model functions. During the experimental run, the subjects were asked to press keyboard buttons "←" and "→" to move the lateral terminator t_T of the test interval into a position that makes both stimulus parts perceptually equal in length (Fig. 2). The physical difference between the lengths of the test and reference intervals, $T - R$, was considered as the value of the illusion magnitude. A single button push varied the position of the terminator by one pixel, which corresponded to approximately 0.5 arcmin. The initial length differences between the stimulus intervals were randomized and distributed evenly within a range of ±10 arcmin.

The subjects were instructed to maintain their gaze on the central stimulus terminator; however, observation time was not limited, and subjects' eye movements were not registered. A combination of two types of stimulus presentation conditions was used in each experimental run. In the first condition, the reference (i.e., filled) interval was presented on the left side of the stimulus, whereas in the second condition, the reference was on the right side. Trials from different conditions were randomly interleaved and averaged in order to minimize effects of the left/right visual field anisotropy and reduce stimulus persistence. An experimental run consisted of 124 stimulus presentations. In total, 31 different values of the independent variable for each stimulus condition were presented twice each, in a pseudo-random order. Each observer carried out at least five experimental runs on different days. Ten trials contributed to each data point analysis, and in the data graphs, the error bars depict ± one standard error of the mean (SEM).

Subjects

Data were collected from seven human observers, ranging in age from 19 to 28 years (4 males, 3 females). Subjects were naive with respect to the purpose of the study, with the exception one of the authors (V.M.), and all had normal or corrected-to-normal vision. To provide more strict viewing conditions and eliminate potential effects related to binocularity, the right eye was always tested irrespective of whether it was the leading eye or not. All subjects gave their informed consent before taking part in the experiments performed, in accordance with the ethical standards of the Declaration of Helsinki.

RESULTS

In the first series of experiments, we determined the magnitude of the cFSI as a function of the length of a single distracting-line placed outside the reference spatial interval (Fig. 2A). As can be seen from the graphs in Fig. 6, despite relatively large inter-individual differences, the experimental results from all subjects yielded curves of a similar simple shape. We found that the magnitude of the illusion increased relatively smoothly, with the line-segment lengthening up to about one-third of the length of the reference interval with little variability afterwards.

In order to estimate the general trend of the results for the whole group of observers, grand-mean curves (Fig. 6, solid lines) were calculated using the individual experimental data. We found relatively small SEM values for the grand-means, for e.g., not exceeding 0.31, 0.54, and 0.58 arcmin for stimuli with the length of the reference interval equal to 30, 60, and 90 arcmin, respectively. We assert that these relatively small SEM

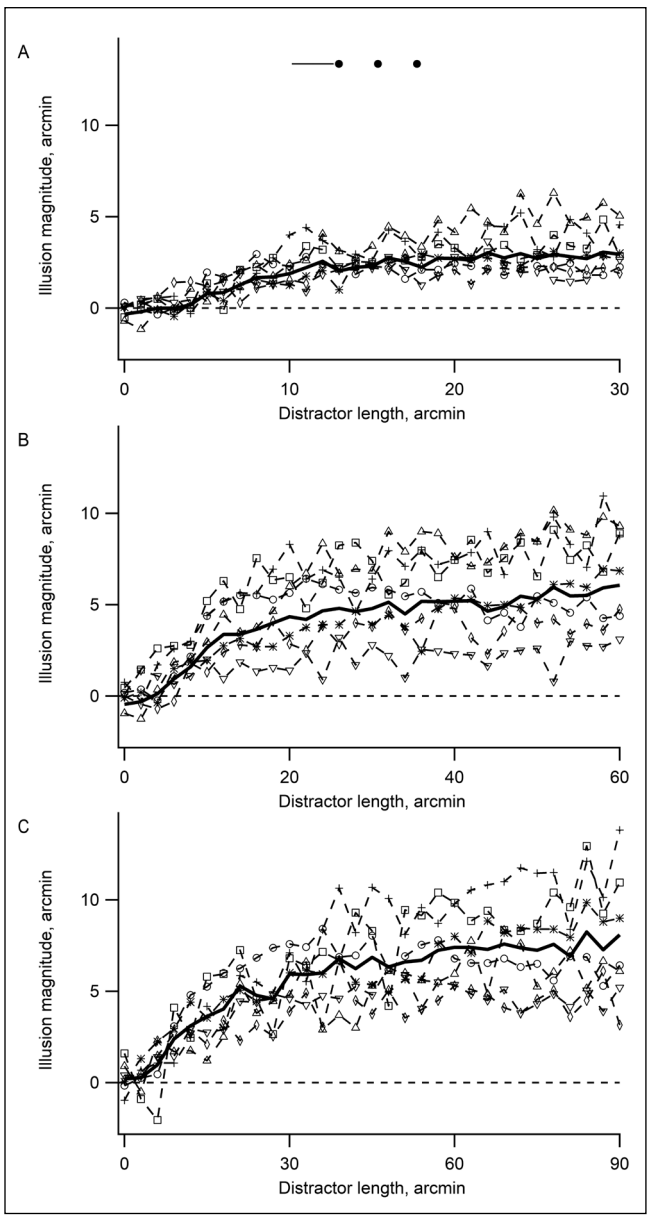

Fig. 6. The illusion magnitude as a function of the length of the distractor attached to the lateral terminator and located outside the reference interval. In the graphs, dashed curves with different symbols represent the individual data for each of the seven subjects. The length of the stimulus reference interval was set to 30 (upper), 60 (middle), and 90 (lower) arcmin. Thick solid curves represent grand-means of the individual data.

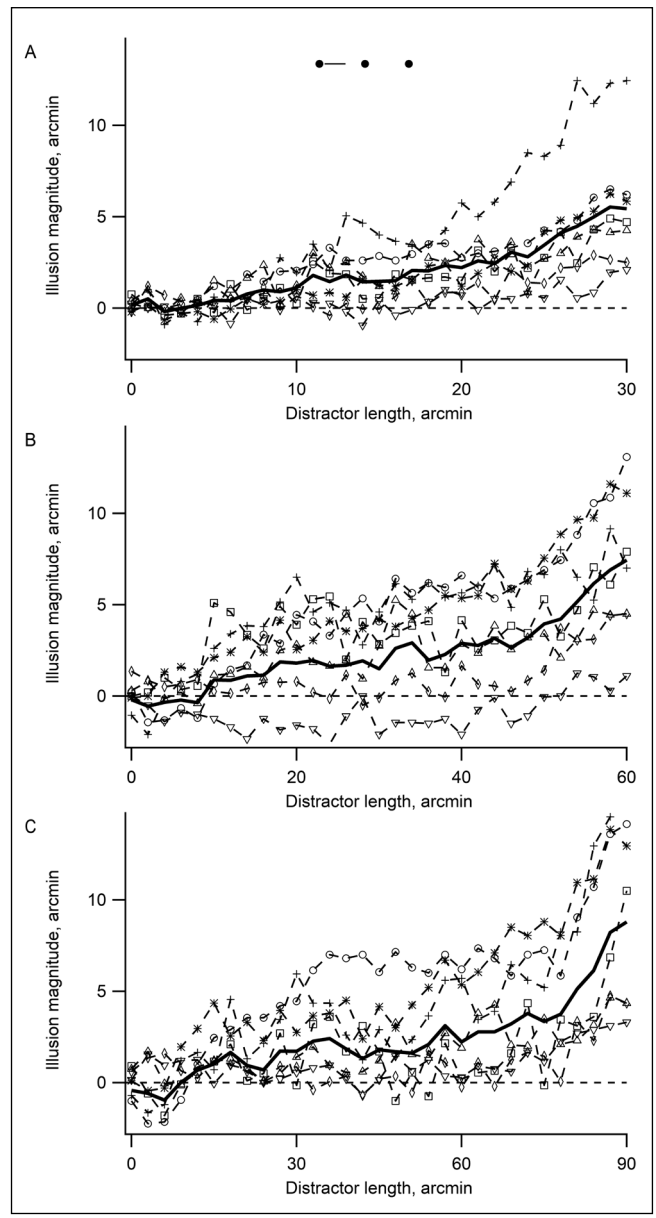

Fig. 7. The illusion magnitude as a function of the length of the distractor attached to the lateral terminator and located inside the reference interval. In the graphs, dashed curves with different symbols represent the individual data for each of the seven subjects. The length of the stimulus reference interval was set to 30 (upper), 60 (middle), and 90 (lower) arcmin. Thick solid curves represent grand-means of the individual data.

values support our assumptions regarding the similarity in the shape of the individual curves.

In the second series of experiments, the endpoint of a single distracting line-segment was attached to the lateral terminator inside the stimulus reference interval (Fig. 2B). Within that interval, the distractor's length varied randomly in a range from zero to the length of the interval. According to the model predictions, it was expected that the shape of the experimental curves should become more complex because of the appearance of additional effects related to perceptual biases of the central stimulus terminator. As can be seen from the graphs in Fig. 7, for most of the subjects, the illusion magnitude increased and saturated for distractors that are shorter than about two-thirds of the length of the stimulus reference interval. This was similar to what was observed in the first series of experiments, although of note, one subject demonstrated

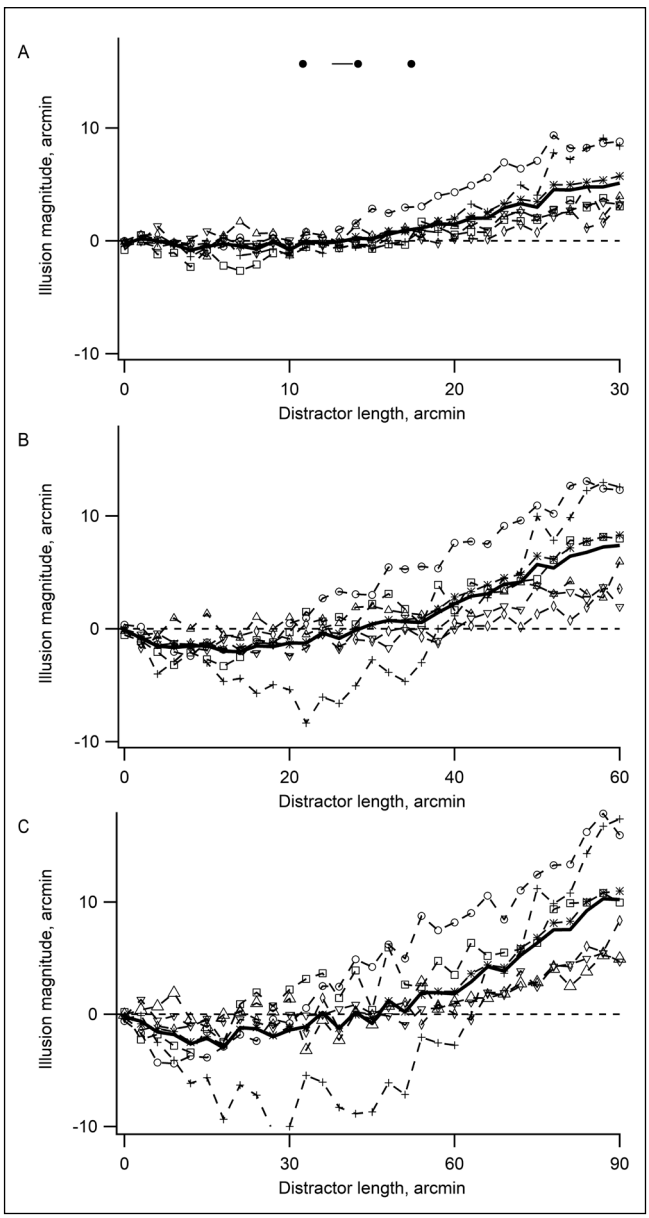

Fig. 8. The illusion magnitude as a function of the length of the distractor attached to the central terminator and located inside the reference interval. In the graphs, *dashed* curves with different symbols represent the individual data for each of the seven subjects. The length of the stimulus reference interval was set to 30 (upper), 60 (middle), and 90 (lower) arcmin. Thick solid curves represent grand-means of the individual data.

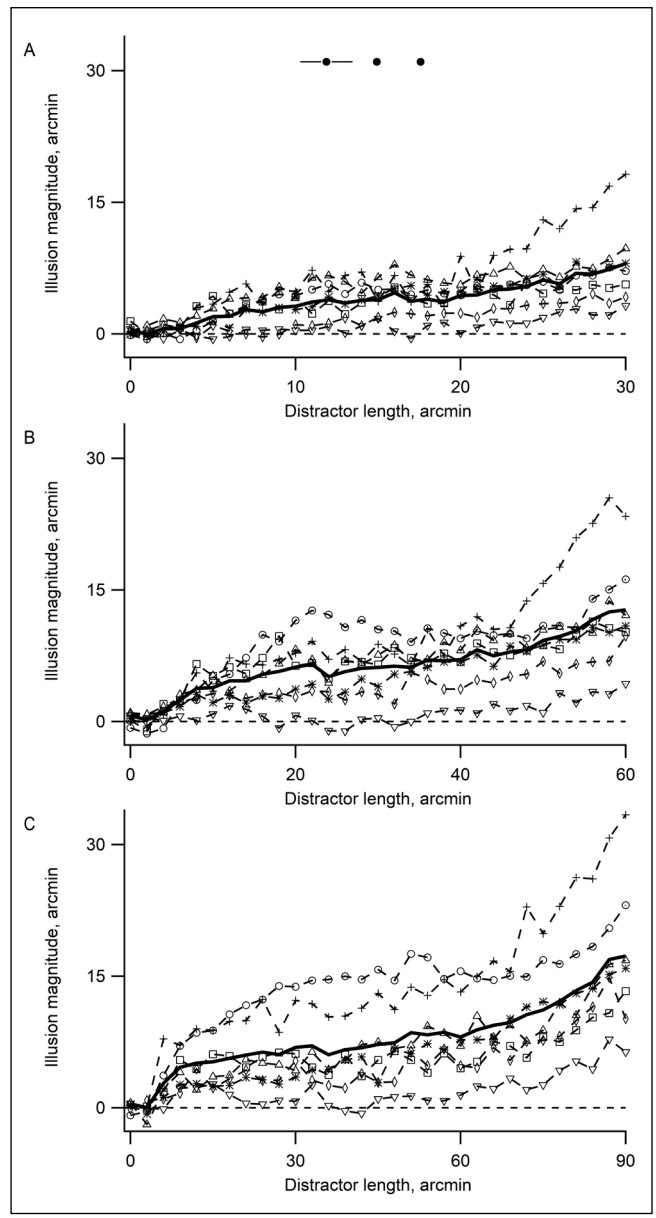

Fig. 9. The illusion magnitude as a function of the length of distractors arranged symmetrically relative to the lateral terminator. In the graphs, dashed curves with different symbols represent the individual data for each of the seven subjects. The length of the stimulus reference interval was set to 30 (upper), 60 (middle), and 90 (lower) arcmin. Thick solid curves represent grand-means of the individual data.

negative illusion values. However, a further increase of the distractor length until the complete filling of the reference interval caused a considerable strengthening of the illusion. Similar to what was observed in the previous series of experiments, the regularities described can be more easily seen in the grand-mean curves calculated from the individual data of the entire group of observers (Fig. 7, solid lines). In the grand-means, the SEM values do not exceed 0.63, 0.77, and 0.89 arcmin for the reference interval lengths of 30, 60, and 90 arcmin, respectively.

In the third series of experiments, we used stimuli (Fig. 2C) with a single distractor attached to the central terminator instead of the lateral terminator. The latter was the only difference compared with the previous series, but the results obtained significantly diverged from prior results. As can be seen from the graphs in Fig. 8, data for most of the subjects revealed a region

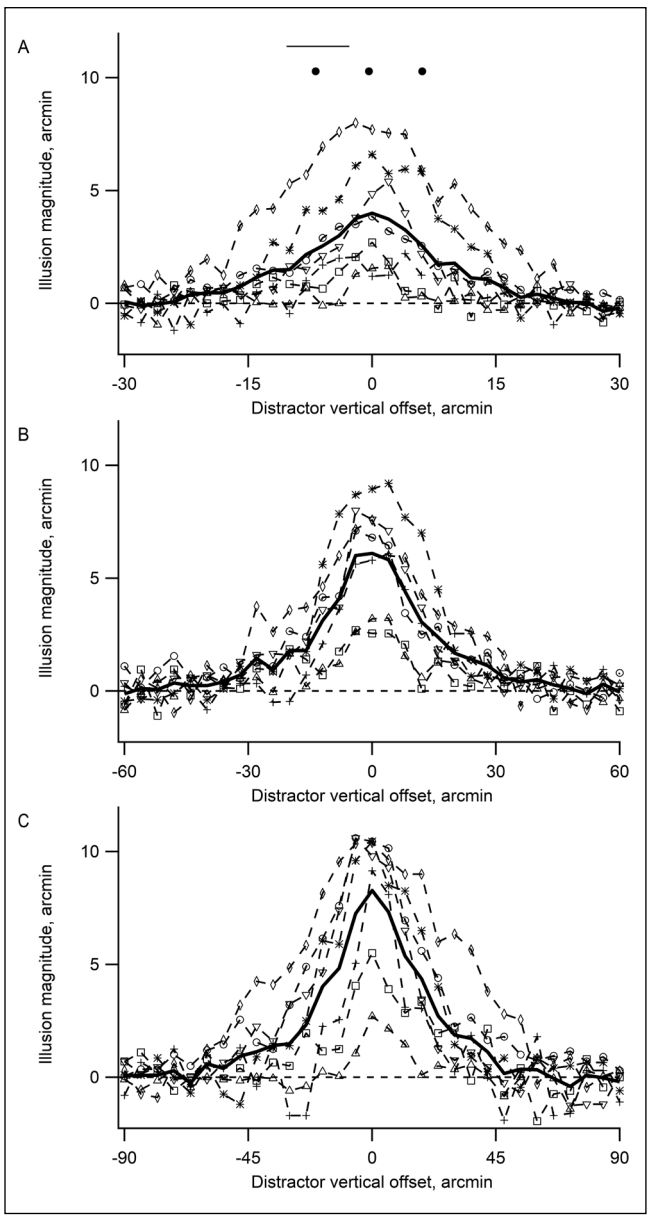

Fig. 10. The illusion magnitude as a function of the vertical offset of distractors. In the graphs, dashed curves with different symbols represent the individual data for each of the seven subjects. The length of the stimulus reference interval was set to 30 (upper), 60 (middle), and 90 (lower) arcmin. Thick *solid* curves represent grand-means of the individual data.

with well-expressed negative values of the illusion magnitude. This region was observed for distractors that ranged in length from zero to about one-third or the half of the reference interval. However, the elongation of distractors until they fill the entire reference interval gives values of the illusion similar to those obtained in the second series of experiments. The values of SEM for the grand-mean curves (Fig. 8, solid lines) do not exceed 0.53, 0.72, and 0.95 arcmin for reference interval lengths of 30, 60, and 90 arcmin, respectively. These data suggest, to some extent, a similarity in the individual experimental data sets.

In the fourth series of experiments, two distracting line-segments arranged symmetrically with respect to the lateral stimulus terminator were used (Fig. 2D). In these experiments, the length of the distractors varied randomly from zero to the length of the reference interval. As expected based on our model predictions, for all the subjects the experimental data yielded curves (Fig. 9) that were similar in shape to those obtained in the second series of experiments. Indeed, the magnitude of the illusion was approximately equal to the sum of relevant values obtained in the first and second series. The SEM values for the grand-mean curves (Fig. 9, solid lines) did not exceed 0.7, 0.98, and 1.27 arcmin for reference interval lengths of 30, 60, and 90 arcmin, respectively.

The purpose of the fifth series of experiments was to test the model's assumption regarding the parameters of the weighted summation along the vertical dimension of the AWS. As can be seen from the graphs in Fig. 10, for all the subjects, the experimental data yielded bell-shaped curves that were similar to Gaussian functions. As was observed in the previous series of experiments, the described patterns were easier to see in the grand-mean curves calculated from the individual data of the entire group of observers (Fig. 10, solid lines). The SEM values in the grand-mean curves did not exceed 0.4, 0.47, and 0.64 arcmin for reference interval lengths of 30, 60, and 90 arcmin, respectively. Of note, we obtained relatively similar illusion values for same set of stimulus parameters (i.e., zero vertical offsets of the distractors, with length equal to 0.5*R*) in the fifth and fourth series of experiments. Indeed, paired samples *t*-test, *df*=6, α=0.05: *t30*=0.113 [*P*=0.914], *t60*=0.118 [*P*=0.91], and *t90*=0.59 [*P*=0.577] for stimulus reference interval lengths of 30, 60, and 90 arcmin, respectively. These results provide additional support for the relatively good precision of our experimental measurements.

Theoretical assessment of the illusion parameters is associated with a considerable number of observer-specific factors regarding the actual gaze direction and scaling the size of relevant AWSs, which can essentially affect the accuracy of the model predictions. Therefore, to identify the most common regularities in the body of data gathered in experiments, the grand-mean curves calculated from the individual results for the entire group of the observers were submitted to quantitative analysis. In addition, to reduce the number of free parameters of the model functions, we used several sequential steps to fit the data from different series of experiments. Since the smallest number of influencing factors corresponds to the data collected

in the first series of experiments (i.e, with a single external distractor), we used the following function to fit these data (Fig. 11, upper row). This function has three free parameters (k, Ω, and C):

$$I(d,k,\Omega,C) = C + \frac{\sqrt{QL_{out}(d,\Omega)} - \sqrt{\pi}\Omega}{k\sqrt{\pi}}, \quad (12)$$

where C refers to a constant shift along the ordinate axis, k is the slope of linear regression in formula 1, and Ω refers to the standard deviation of the Gaussian profile of AWS centered at the lateral terminator t_R. That is, Function 12 corresponds to Function 11 but with coefficient β=0, because the increase of cumulative response of only the "lateral" window theoretically determines the occurrence of the illusion.

The method of least squares with the implementation of sequential quadratic programming algorithm (LeastSquaresFit function, Mathcad, Parametric Technology Corporation) was used to fit the experimental data. The results (Table I) of fitting of the data from the first series of experiments allowed us to calculate

Table I. The resulting parameters of fitting model functions to experimental data.[1]

Location of terminator, distractor	Parameters	The length of the reference interval, *arcmin*		
		30	60	90
Lateral, outside (Fig. 2A)	C	-0.15±0.21	-0.22±0.54	0.78±0.7
	k	0.2±0.03	0.15±0.03	0.23±0.05
	Ω	5.72±0.55	8.12±1.04	14.25±2.02
	R^2	0.96	0.94	0.92
	W, P_w	0.96, 0.35	0.96, 0.33	0.97, 0.64
Lateral, inside (Fig. 2B)	C	-0.31±0.2	-0.98±0.34	-1.4±0.45
	γ	0.5±0.09	0.42±0.08	0.3±0.06
	β	1±0.19	0.58±0.11	0.3±0.05
	R^2	0.93	0.92	0.91
	W, P_w	0.98, 0.88	0.96, 0.31	0.97, 0.52
Central, inside (Fig. 2C)	C	0.09±0.62	-0.23±0.73	-0.39±1.06
	γ	1.31±0.19	1.24±0.08	1.1±0.07
	β	-0.18±0.28	-0.31±0.21	-0.55±0.63
	R^2	0.93	0.97	0.95
	W, P_w	0.96, 0.22	0.97, 0.44	0.95, 0.15
Lateral, symmetrical (Fig. 2D)	C	0.04±0.25	0.35±0.41	0.37±0.68
	γ	0.53±0.07	0.44±0.05	0.33±0.05
	β	1±0.17	0.82±0.11	0.7±0.09
	R^2	0.95	0.96	0.95
	W, P_w	0.96, 0.23	0.97, 0.53	0.95, 0.16
Lateral, shifted vertically (Fig. 2E)	C	0.16±0.2	0.38±0.22	0.34±0.31
	γ	0.53±0.04	0.42±0.03	0.41±0.03
	R^2	0.92	0.94	0.93
	W, P_w	0.97, 0.59	0.97, 0.44	0.99, 0.95

[1] C (*arcmin*), a constant component; k, the slope specifying eccentricity scaling for the standard deviation of the Gaussian profile of AWS; Ω (*arcmin*), the standard deviation of the Gaussian profile of the lateral AWS; γ, coefficient determining the position of gaze fixation; β, coefficient determining the contribution of the central AWS; R^2, coefficient of determination; W and P_w, the Shapiro-Wilk test statistic and *p-value*, respectively.

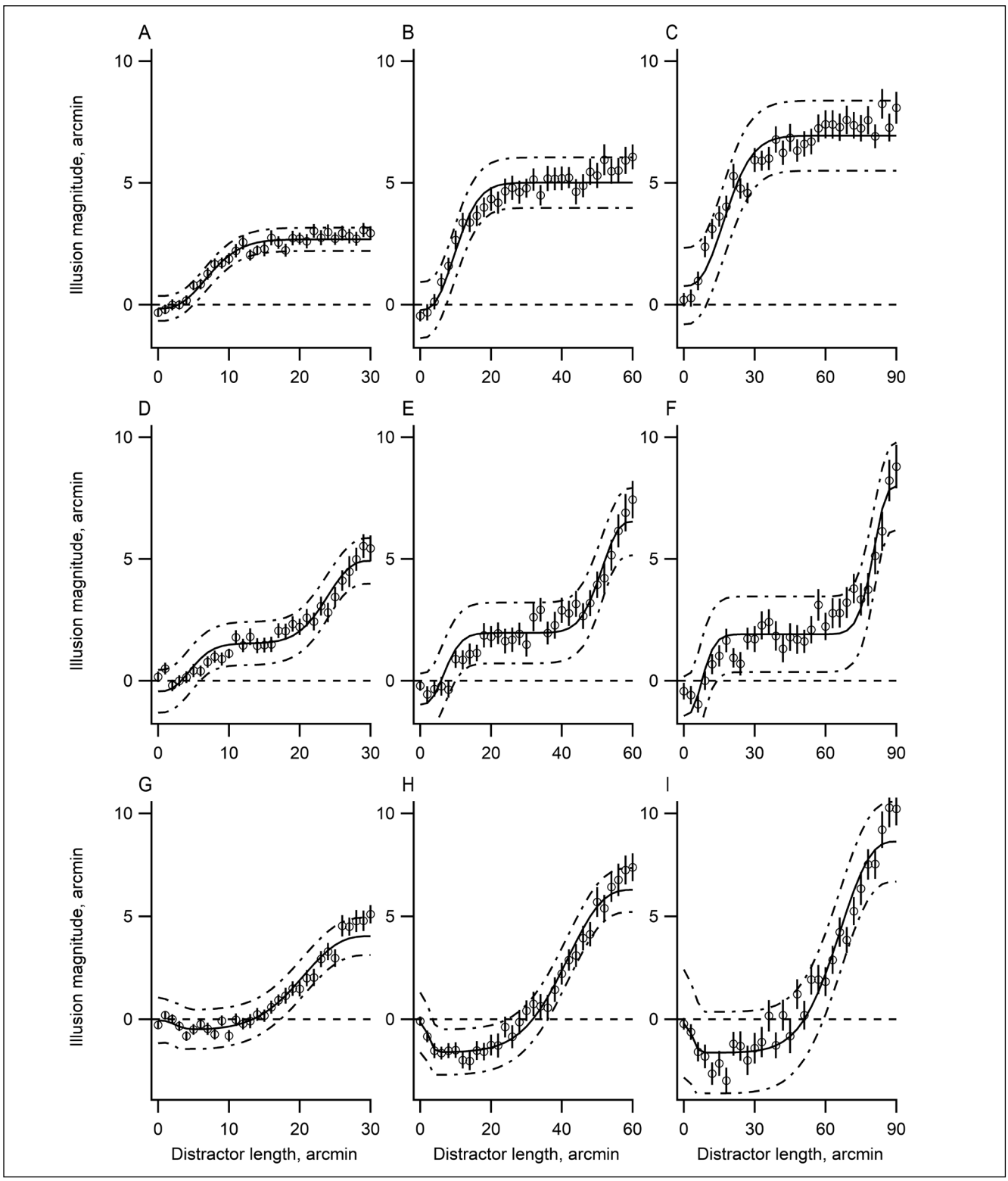

Fig. 11. The results of the fitting of the model functions to the data from the first to the third series of experiments. In the graphs, open circles represent grand-means (from Fig. 6 - 8) of the individual data for all seven subjects as a function of the distractor length. The size of the stimulus reference interval was set to 30 (left column), 60 (middle column), and 90 (right column) arcmin. The following stimuli were used to generate data shown in each row: upper, the distractor attached to the lateral terminator from outside the reference interval (Fig. 2A); middle, the distractor attached to the lateral terminator from inside the reference interval (Fig. 2B); lower, the distractor attached to the central terminator (Fig. 2C). Solid curves represent the least squares fitting of the model functions to the experimental data; dash-dot curves represent confidence intervals of the fitting. Error bars depict ± one standard error of the mean (SEM).

an averaged value of the coefficient k=0.193±0.035. Next, we established the parameters of the linear regression of standard deviations Ω of the Gaussian profiles of "lateral" AWS for three different lengths (R) of the stimulus reference interval: $\Omega(R)=0.832 + 0.142R$. The corresponding Pearson's correlation coefficient is equal to 0.97, the standard errors of the estimate, of the intercept, and of the slope are equal to 1.52, 2.32, and 0.036, respectively. Assuming approximately the same appropriately scaled pattern of eye movements during the observations of stimuli of different sizes, it is reasonable to consider the intercept (0.832 arcmin) of this linear regression as the value of the parameter σ_0 in Formula 1. Further, we can estimate the averaged position of gaze fixation using the ratio of slopes $\gamma=0.142/0.193 \approx 0.74$.

In turn, the use of above-established values for k and σ_0 allows the reduction of free parameters to three (γ, β, and C) in the fitting of the model function (Fig. 11, middle and lower rows; Fig. 12, upper row) to the data obtained in experiments. This can be applied to data collected from the second to the fourth series of experiments, with stimuli that are comprised of distractors located inside the reference interval:

$$I(d,\gamma,\beta,C) = C + \frac{\sqrt{QL\left(d,\sigma_\gamma\right)} - \sqrt{S\left(R\gamma\right)}}{k\sqrt{\pi}} + 2\beta\frac{\sqrt{QC\left(d,\sigma_{1-\gamma}\right)} - \sqrt{S\left(R(1-\gamma)\right)}}{k\sqrt{\pi}}, \quad (13)$$

where R represents the length of the reference stimulus interval; $\sigma_\gamma=kR|\gamma| + \sigma_0$ and $\sigma_{1-\gamma}=kR|1-\gamma| + \sigma_0$ represent the standard deviations of the Gaussian profiles of AWS centered at the lateral and at the central terminator, respectively. Thus, Function 13 corresponds to Function 11 with an additional argument (C) that refers to a constant shift along the ordinate axis.

In the case of stimuli with vertically shifted line-segments (Fig. 2E), it seems reasonable to assume – due to relatively short distractors – that only the contribution from the AWS centered at the lateral terminator determines the effect of the illusion (i.e., the coefficient β is equal to zero). Therefore, it is possible to use only two free parameters (γ and C) in the fitting of Function 11 to data collected from the fifth series of experiments (Fig. 12, *lower* row):

$$I(h,\gamma,C) = C + \frac{\sqrt{QL_{off}\left(h,\sigma_\gamma\right)} - \sqrt{S\left(R\gamma\right)}}{k\sqrt{\pi}}, \quad (14)$$

where h represents the vertical offset of distracting line-segments.

The fitting of grand-mean curves demonstrated a good correspondence between the computational and experimental results (Figs 11–12, solid curves). Indeed, the values of the coefficient of determination in all the cases were higher than 0.9 (Table I). Next, we used the Shapiro-Wilk test to perform a more thorough examination of goodness-of-fit (Table I). Shapiro-Wilk test is an assessment of normality of residuals. For each calculated curve, a matrix of partial derivatives of the model's function was multiplied by the residual mean square. These data allowed for an additional evaluation of the goodness-of-fit by calculating confidence intervals for predicted values at each point along the range of the independent variable (Fig. 11–12, dash-dot curves).

According to the model, the data from the fourth series of experiments (i.e., stimuli with two distractors aligned symmetrically relative to the lateral terminator) should be approximately equal to the sum (Fig. 12, upper row, filled circles) of the corresponding illusion magnitudes obtained in the first and the second series of experiments (i.e., stimuli with a single distractor attached to the terminator from outside/inside the reference interval). In order to check this prediction, we applied paired samples t-test (df=30, α=0.05) with a preliminary assessment of normality of residuals, using the Shapiro-Wilk test. As expected, no significant differences were found between the relevant data sets for all stimulus sizes (Shapiro-Wilk test: $W30$=0.959 [P=0.268], $W60$=0.948 [P=0.14], and $W90$=0.986 [P=0.955]; paired samples t-test: $t30$=1.186 [P=0.245], $t60$=0.179 [P=0.859], and $t90$=0.47 [P=0.642] for stimulus reference interval lengths of 30, 60, and 90 arcmin, respectively).

DISCUSSION

The present study aimed to extend the previously proposed (Bulatov et al., 2017; 2019) explanation of the cFSI and to verify whether this theoretical approach is relevant in the case of stimuli that are comprised of distracting line-segments of different lengths and locations. Our results (Figs 11–12; Table I), together with model equations (despite their obvious simplicity), demonstrate that general trends in the illusion manifestation caused by varying stimulus parameters can by accurately described. Thus, it can be con-

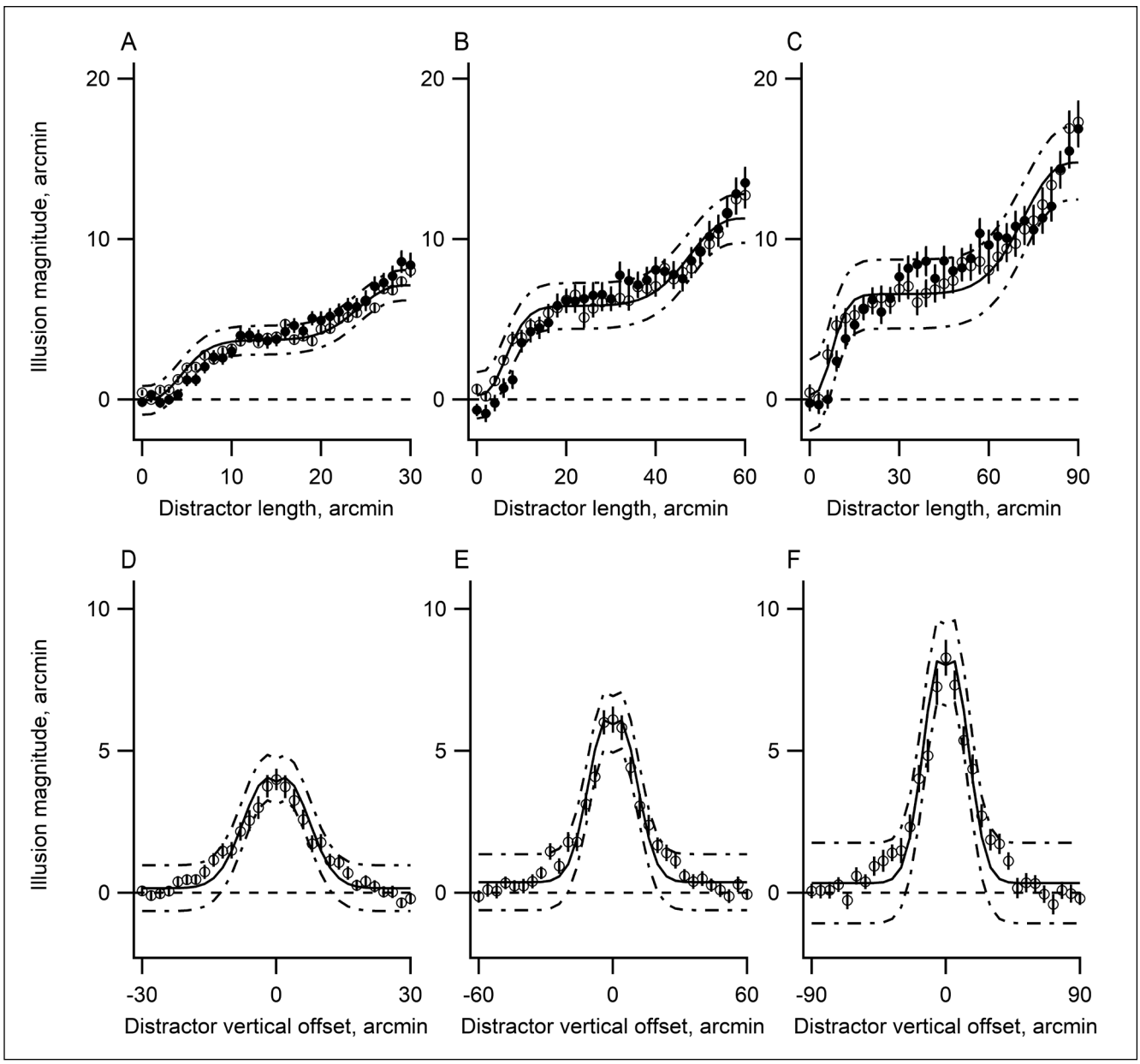

Fig. 12. The results of the fitting of the model functions to the data from the fourth and the fifth series of experiments. In the graphs, open circles represent grand-means (from Fig. 9 - 10) of the individual data for all seven subjects as a function of the distractor length (upper row) or vertical offset (lower row). The size of the stimulus reference interval was set to 30 (left column), 60 (middle column), and 90 (right column) arcmin. The following stimuli were used to generate data shown in each row: upper, two distractors arranged on the stimulus x-axis symmetrically relative to the lateral terminator (Fig. 2D); lower, the distractors shifted in direction orthogonal to the stimulus axis (Fig. 2E). In the upper row, filled circles represent the results of the summation of the corresponding grand-means from the first (Fig. 6) and the second (Fig. 7) series of experiments. Solid curves represent the least squares fitting of the model functions to the experimental data; dash-dot curves represent confidence intervals of the fitting. Error bars depict ± one standard error of the mean (SEM).

cluded that the data gathered in the study are quite consistent with the illusion's explanation based on the assumption that the context-evoked augmentation of neural excitation induces biases in perceptual spatial localization of stimulus terminators. However, it should be emphasized that, because of its extreme simplicity, the proposed explanation does not claim to identify any particular neural mechanism underlying the illusion occurrence. Indeed, our explanation only suggests directions for future research, for e.g., by testing the validity of the model's quantitative predictions. As shown in the derivation of the model equations, the illusion strongly depends on the actual position of gaze fixation during stimulus observation.

This dependence on gaze fixation thereby introduces significant uncertainty in efforts to quantify the illusion magnitude. This feature makes our modeling quite consistent with Robinson's (1998) statement that any successful theory of visual-geometric illusions must necessarily account for effects associated with eye movements and gaze fixation. The presented model is also generally compatible with experimental data showing that gaze fixation in the filled part of the stimulus causes a much stronger illusion than in the case of fixation in an empty spatial interval (Piaget and Bang, 1961). Moreover, as can be seen from the graphs in Fig. 5, the behavior of the illusion (i.e., the shape of curves) does not change dramatically with variations in gaze fixation (values of the coefficients γ and β); thus, the uncertainty caused by these variations is not fundamental and the validity of the model predictions remains unchanged in general. Nevertheless, we consider the lack of direct experimental evidence on the actual pattern of gaze fixations as one of the most important shortcomings of the present study. This limitation should be resolved in future research, for e.g., by using appropriate experimental methods.

We applied several essential simplifications to the model that may cause certain calculation inaccuracies. For example, one of the most important issues is related to the method of normalization of neural activity. According to data presented in the literature (Reynolds and Heeger, 2009; Olsen et al., 2010; Carandini and Heeger, 2012; Vokoun et al., 2014), normalization can be implemented in a variety of neural processes for making neural representations invariant with respect to various stimulus parameters. Normalization is typically described in terms of the so-called divisive normalization, which is the neuronal response is divided by the integrated activity of neighboring neurons in the population. However, given that our current approach represents only an initial step towards a more elaborated quantitative description of the illusion phenomenon, we applied in the model a simple scaling of excitation amplitude between 0 and 1. Another substantial simplification was made in Formula 3 regarding the shape the profile of neural excitation evoked by distracting line-segments. This simplification involved the use of a piecewise-constant function along the stimulus x-axis. Of note, however, the numerical examinations of the model functions have shown that such a substitution has only a negligible effect on the resulting illusion calculations. Further, for simplicity, in model calculations we used a circular shape and the same dimensions of the Gaussian profiles of AWS and relevant neural excitation. We believe that suggestions regarding the shape of the profiles are largely supported by the results from the fifth series of experiments. However, the methods of the present study allowed us to establish only approximate integral characteristics of the AWS in the direction orthogonal to the stimulus axis; thus, the problem regarding a more detailed spatial structure of its two-dimensional weighting profile remains largely unresolved and should be examined more thoroughly in future cFSI studies.

A wide variety of other related factors were not accounted for in the model, which can significantly influence the assessment of the parameters of the cFSI. For example, complex processes of perceptual grouping in higher-order visual regions that likely affect the length judgements (Noguchi et al., 1990; Noguchi, 2003; Tannazzo et al., 2014) remained beyond the scope of the present modeling. Model calculations also did not concern the processes of spatial differentiation caused by two-dimensional spatial-frequency filtering, which occurs even at the lowest hierarchical levels of visual processing. Due to this filtering, the regions of edges in the stimulus-evoked excitation patterns become strongly emphasized. This results in, for example, contour-line extraction because of abrupt changes in luminance, which substantially strengthens the similarity between the excitation profiles evoked by the outlined and uniformly filled patterns that have the same contour-shape. This feature may explain the practical absence of differences between the results from experiments with uniformly filled and outlined two-dimensional shapes (Bulatov et al., 2015). Filtering effects are not essential for the one-dimensional stimuli of the current study but should be accounted for when trying to analyze the data obtained with two-dimensional patterns. For example, filtering effects can be more noticeable in stimuli used, for example, in studies Botti (1906) or Giora and Gori (2010).

Regarding the possible manifestation of attentional bias caused by relatively more salient distracting lines, we believe that there are several arguments supporting the reliability of the obtained experimental data. First, the stimuli used in the second and third series of experiments (i.e., distracting line-segments attached to the lateral and the central terminator, respectively) are quite symmetrical with respect to their ability to provoke the attentional bias under consideration. Therefore, in the case of a noticeable bias, a significant similarity of the corresponding experimental data could be expected. However, the experimental curves from the graphs shown in Fig. 11 demonstrate a considerable difference between the results of the second and third series of experiments. Moreover, the differences observed in these data can be rather successfully ap-

proximated by relevant functions of the model. Second, we believe that the general consistency of experimental data collected with different naïve subjects during experimental runs performed on different days also confirms, to some extent, the reliability of our results. In this regard, attention should be paid to the fact that the illusion magnitude established in the fourth series of experiments is almost equal to the sum of relevant values obtained in the first and second series of experiments. That is, the obtained data are in good agreement with the model predictions. Notwithstanding these observations, we propose that future cFSI studies should compensate for possible attentional bias, by using stimuli with a completely filled (by the shaft-line) test spatial interval.

Fitting the model to the current experimental data yielded quite reasonable values of the slope (k=0.193) and the intercept (σ_0=0.832 arcmin) of the linear dependence of the standard deviation σ of the Gaussian profile of AWS on visual field eccentricity. For instance, the calculated sizes of AWS (4×σ) are equal to about 3.3 and 49.7 arcmin at eccentricity 0 and 60 arcmin, respectively. These AWS sizes agree rather well with data reported in the literature regarding the spatial resolution of visual attention (Nakayama and Mackeben, 1989; Intriligator and Cavanagh, 2001). Current assessments of dimensions of the AWS (35.8 and 68.2 arcmin) are also quite consistent with averaged widths (33.1 and 64.2 arcmin) of the areas of the automatic centroid extraction that are located at eccentricities of 42 and 84 arcmin, respectively. These widths were obtained in experiments with stimuli that are comprised of closed two-dimensional shapes from our previous study of the Brentano illusion (Bulatov et al., 2015). However, it should be noted that, although the value of the slope (k=0.19±0.01) from our previous investigation of the cFSI evoked by single-dot distractors (Bulatov et al., 2019) is in remarkably good agreement with that established in the present study, the estimates of the intercept (5.96 *vs.* 0.832 arcmin) differ significantly. We believe that such a large discrepancy can be explained by a relatively low sensitivity to variations in the intercept value for the least-squares procedure of fitting model functions to the experimental data. In addition the discrepancy may arise from the fact that, in our previous study, we used only one stimulus size with reference interval length equal to 60 arcmin. Thus, significantly different methods were used to estimate the intercept between our previous work and the current study.

It is important to note that our estimates of AWS scaling with eccentricity are largely in agreement with relevant parameters of critical spacing in the pooling regions of crowding. Crowding is a perceptual phenomenon that reflects a failure of visual discrimination of an object because of the influence of nearby flankers. Previous studies of visual crowding in humans (Levi, 2008; Strasburger et al., 2011; Whitney and Levi, 2011; Wallis and Bex, 2012; Strasburger and Malania, 2013) have demonstrated that this critical spacing scales with visual eccentricity with a factor in a range approximately from 0.3 to 0.7. Of note, the value of the spacing factor depends strongly on how the separation between the target and the flankers is determined across different studies. For comparison, if we take as the criterion of the minimum separation between the target and the flanker two standard deviations that specify their Gaussian profiles, then the calculation (2×k) of the scale factor for grand-mean data from our current study yields a value of about 0.39. Importantly, this value closely matches the estimate (0.34±0.09) of the corresponding slope established in the previous study of the Brentano illusion evoked by stimuli composed of separate dots (Bulatov et al., 2010). However, it should be stressed that the above comparisons concern only issues of spatial scaling across retinal eccentricity, and do not imply any common base for neural mechanisms underlying different types of illusions and crowding.

Unfortunately, to our knowledge, there are no other experimental or quantitatively developed theoretical studies of the cFSI. Therefore, a direct comparison of the present model with other explanations devoted to this topic seems rather complicated. However, we can assume some affinity between the cFSI and the Oppel-Kundt illusion. Based on this comparison, we can consider an alternative way of interpreting the experimental data collected for the present study; namely, the notion that visual geometric illusions are based on the crucial role of effects caused by spatial-frequency filtering performed by receptive fields of neurons at different levels of the visual system (Ginsburg, 1986; Morgan et al., 1990; Bulatov et al., 1997; Morgan, 1999; Surkys et al., 2006; Sierra-Vázquez and Serrano-Pedraza, 2007; Bulatov et al., 2009). According to this approach, illusory effects appear as a result of the filtering-induced metrical distortions of the profile of neural activity (i.e., that physically change distances between specific loci, for example, peaks). Thus, this explanation implicitly assumes the existence of a certain higher-level neural mechanism that is responsible for comparing these distances. For instance, the emergence of the Oppel-Kundt illusion can be related to the processes of lateral inhibition (Ganz, 1966; Blakemore et al., 1970), which cause the peaks of excitation evoked by contextual fillers to be slightly shifted apart from each other. The shifting of the peaks, in turn, may result in the emergence of the illusion due to perceptual repulsion of stimulus elements. Additionally, prior data – although rather contradictory – suggest that the effects

of repulsion are not sufficient for accounting for the actual strength of the Oppel-Kundt illusion (Rentschler et al., 1975; Mikellidou and Thompson 2014). Nevertheless, even if this "repulsion" explanation could be granted for the Oppel-Kundt figures comprising separate contextual fillers, it is unclear whether this theory provides a relevant basis to account for the results with stimuli used in the present study. Further, theories that are based on the idea of the filtering-induced metrical distortions of the profile of excitation offer no explanation as to why the illusion magnitude practically doubles in the case wherein two distractors are symmetrically attached (Fig. 2D) to the lateral terminator. In contrast, the approach we outline here provides a rather simple unified interpretation of the experimental results. Our approach relies on the assumption that the illusion emerges due to the context-evoked augmentation of the cumulative neural response of the relevant AWS. In addition, our modeling offers some suggestions concerning the aforementioned hypothetical neural mechanism responsible for comparing distances within the excitation profile (i.e., by specifying mutual coordinates of different loci). Therefore, we believe that the proposed computational principles can also be used to account for the effects of well-known illusions of the Müller-Lyer type via relevant modifications of input parameters to the proposed model of the cFSI.

Given the basic initial assumptions of the model and correspondence between theoretical predictions and experimental data from our current and previous investigations (Bulatov et al., 2017; 2019), we hypothesize that visual information processing in the superficial layers of the superior colliculus – along with cortical areas (e.g., frontal eye fields and functional equivalents of macaque area LIP in human parietal cortex) – can largely be associated with the phenomenon under study. It is widely accepted (Klier et al., 2001; Bergeron et al., 2003; Nakahara et al., 2006; Katyal et al., 2010; Hafed et al., 2013; Krauzlis et al., 2013; Vokoun et al., 2014; Taouali et al., 2015; Bremmer et al., 2016) that these brain regions are directly involved in neural encoding of information on the retinotopic localization of visual objects, and that these regions play an important role in the control of spatial attention and gaze fixations.

Since the stimuli used in our experiments were composed of simple homogeneous elements that possess the same horizontal orientation, the results obtained cannot be immediately extended to more general conditions with stimuli of different orientations containing contextual two-dimensional forms. Further studies are needed to verify whether the same principles in the interpretation of perceptual misjudgments can be used in the case of more sophisticated filling with varied luminance distribution.

CONCLUSIONS

In the present study, we further extended the computational model of the cFSI based on the assumption that length judgments are associated with neural calculations of retinal coordinates of stimulus elements. The model predictions were verified in four series of psychophysical experiments with distracting line-segments attached to different endpoints of the reference spatial interval of the three-dot stimulus. The assumption regarding the parameters of the two-dimensional Gaussian profile of hypothetical areas of weighted spatial summation was tested in experiments with distractor shifts in the direction orthogonal to the stimulus axis. Collected experimental data were fit to the model functions by using the least squares method with the implementation of sequential quadratic programming. A good correspondence between the computational and experimental results supports the suggestion that the context-evoked increase in neural excitation induces perceptual positional biases in the stimulus terminators, thus causing the illusion under consideration.

REFERENCES

Bailes SM (1995) Effects of processing time and stimulus density on apparent width of the Oppel-Kundt illusion [Ph.D. Thesis]. Concordia University, Montréal, QC, CA.

Bergeron A, Matsuo S, Guitton D (2003) Superior colliculus encodes distance to target, not saccade amplitude, in multi-step gaze shifts. Nat Neurosci 6: 404–413.

Bertulis A, Bulatov A (2001) Distortions of length perception in human vision. Biomedicine 1: 3–23.

Bertulis A, Surkys T, Bulatov A, Bielevičius A (2014) Temporal dynamics of the Oppel-Kundt illusion compared to the Müller-Lyer illusion. Acta Neurobiol Exp 74: 443–455.

Blakemore C, Carpenter RHS, Georgeson MA (1970) Lateral inhibition between orientation detectors in the human visual system. Nature 228: 37–39.

Botti L (1906) A contribution to the knowledge of variable geometric-optical illusions of extend (in German). Archiv für die gesamte Psychologie 6: 306–315.

Bremmer F, Kaminiarz A, Klingenhoefer S, Churan J (2016) Decoding target distance and saccade amplitude from population activity in the macaque Lateral Intraparietal Area (LIP). Front Integrat Neurosci 10: 30.

Bulatov A, Bertulis A (2005) Superimposition of illusory patterns with contrast variations. Acta Neurobiol Exp 65: 51–60.

Bulatov A, Bertulis A, Mickienė L (1997) Geometrical illusions: study and modelling. Biol Cybern 77: 395–406.

Bulatov A, Bertulis A, Bulatova N, Loginovich Y (2009) Centroid extraction and illusions of extent with different contextual flanks. Acta Neurobiol Exp 69: 504–525.

Bulatov A, Bertulis A, Gutauskas A, Mickienė L, Kadzienė G (2010) Center-of-mass alterations and visual illusions of extent. Biol Cybern 102: 475–487.

Bulatov A, Bulatova N, Loginovich Y, Surkys T (2015) Illusion of extent evoked by closed two-dimensional shapes. Biol Cybern 109: 163–178.

Bulatov A, Bulatova N, Surkys T, Mickienė L (2017) An effect of continuous contextual filling in the filled-space illusion. Acta Neurobiol Exp 77: 157−167.
Bulatov A, Marma V, Bulatova N, Mickienė L (2019) The filled-space illusion induced by a single-dot distractor. Acta Neurobiol Exp 79: 39−52.
Carandini M, Heeger DJ (2012) Normalization as a canonical neural computation. Nat Rev Neurosci 13: 51−62.
Coren S, Hoenig P (1972) Eye movements and decrement in the Oppel-Kundt illusion. Percept Psychophys 12: 224−225.
Coren S, Girgus JS, Ehrlichman H, Hakistan AR (1976) An empirical taxonomy of visual illusions. Percept Psychophys 20: 129−147.
Craven BJ, Watt RJ (1989) The use of fractal image statistics in the estimation of lateral spatial extent. Spat Vis 4: 223−239.
Deregowski JB, McGeorge P (2006) Oppel-Kundt illusion in three-dimensional space. Perception 35: 1307−1314.
Dumoulin SO, Wandell BA (2008) Population receptive field estimates in human visual cortex. Neuroimage 39: 647−660.
Dworkin L, Bross M (1998) Brightness contrast and exposure time effects on the Oppel-Kundt illusion. Perception 27: 87.
Erdfelder E, Faul F (1994) A class of information integration models for the Oppel-Kundt illusion (in German). Zeitschrift für Psychologie 202: 133–160.
Eriksson ES (1970) A field theory of visual illusions. Br J Psychol 61: 451−466.
Field DJ, Hayes A, Hess RF (1993) Contour integration by the human visual system: Evidence for a local "association field". Vis Res 33: 173–193.
Ganz L (1966) Mechanism of the figural aftereffects. Psychol Rev 73: 128–150.
Ginsburg AP (1986) Spatial filtering and visual form perception. In: Boff KR, Koufman L, Thomas JP (Eds.) Handbook of perception and human performance, 34, Wiley and Sons, New York, pp 1–41.
Giora E, Gori S (2010) The perceptual expansion of a filled area depends on textural characteristics. Vis Res 50: 2466–2475.
Graf ABA, Andersen RA (2014) Inferring eye position from populations of lateral intraparietal neurons. Elife 3: e02813.
Hafed ZM, Lee P, Lovejoy LP, Krauzlis RJ (2013) Superior colliculus inactivation alters the relationship between covert visual attention and microsaccades. Eur J Neurosci 37: 1169–1181.
Hirsch J, DeLaPaz RL, Relkin NR, Victor J, Kim K, Li T, Borden P, Rubin N, Shapley R (1995) Illusory contours activate specific regions in human visual cortex: evidence from functional magnetic resonance imaging. Proc Natl Acad Sci USA 92: 6469–6473.
Intriligator J, Cavanagh P (2001) The spatial resolution of visual attention. Cogn Psychol 43: 171−216.
Katyal S, Zughni S, Greene C, Ress D (2010) Topography of covert visual attention in human superior colliculus. J Neurophysiol 104: 3074–3083.
Klier EM, Wang H, Crawford JD (2001) The superior colliculus encodes gaze commands in retinal coordinates. Nat Neurosci 4: 627–632.
Kojo I, Liinasuo M, Rovamo J (1993) Spatial and temporal properties of illusory figures. Vis Res 33: 897–901.
Krauzlis RJ, Goffart L, Hafed ZM (2017) Neuronal control of fixation and fixational eye movements. Philos Trans R Soc B Biol Sci 372: 20160205.
Krauzlis RJ, Lovejoy LP, Zènon A (2013) Superior colliculus and visual spatial attention. Ann Rev Neurosci 36: 165–182.
Levi DM (2008) Crowding – An essential bottleneck for object recognition: A mini-review. Vis Res 48: 635–654.
Lewis EO (1912) The illusion of filled space. Br J Psychol 5: 36–50.
Long GM, Murtagh MP (1984) Task and size effects in the Oppel–Kundt and irradiation illusions. J General Psychol 111: 229–240.
Mikellidou K, Thompson P (2014) Crossing the line: estimations of line length in the Oppel-Kundt illusion. J Vision 14: 20.
Morgan MJ (1999) The Poggendorff illusion: a bias in the estimation of the orientation of virtual lines by second-stage filters. Vis Res 39: 2361−2380.
Morgan MJ, Hole GJ, Glennerster A (1990) Biases and sensitivities in geometrical illusions. Vis Res 30: 1793−1810.
Morgan MJ, Melmoth D, Solomon JA (2013) Linking hypotheses underlying Class A and Class B methods. Vis Neurosci 30: 197–206.
Nakahara H, Morita K, Wurtz RH, Optican LM (2006) Saccade-related spread of activity across superior colliculus may arise from asymmetry of internal connections. J Neurophysiol 96: 765–774.
Nakayama K, Mackeben M (1989) Sustained and transient components of focal visual attention. Vis Res 29: 1631−1647.
Noguchi K (2003) The relationship between visual illusion and aesthetic preference – an attempt to unify experimental phenomenology and empirical aesthetics. Axiomathes 13: 261–281.
Noguchi K, Hilz R, Rentshler I (1990) The effect of grouping of adjacent contours on the Oppel-Kundt illusion. Jpn J Psychon Sci 8: 57–60.
Obonai T (1933) Contributions to the study of psychophysical induction: III. Experiments on the illusions of filled space. Jpn J Psychol 8: 699–720.
Olsen SR, Bhandawat V, Wilson RI (2010) Divisive normalization in olfactory population codes. Neuron 66: 287–299.
Piaget J, Osterrieth PA (1953) Research on the development of perceptions: XVII. The evolution of the Oppel-Kundt illusion as a function of age (in French). Archives de Psychologie 34: 1–38.
Piaget J, Bang V (1961) The evolution of the illusion of divided extent (Oppel-Kundt) in the tachistoscopic presentation (in French). Archives de Psychologie 38: 1–21.
Rentschler I, Hilz R, Grimm W (1975) Processing of positional information in the human visual system. Nature 253: 444−445.
Reynolds JH, Heeger DJ (2009) The normalization model of attention. Neuron 61: 168–185.
Robinson JO (1998) The psychology of visual illusion. Dover Publications, New York, USA.
Sereno AB, Lehky SR (2011) Population coding of visual space: comparison of spatial representations in dorsal and ventral pathways. Front Comput Neurosci 4: 159.
Sierra-Vázquez V, Serrano-Pedraza I (2007) Single-band amplitude demodulation of Müller-Lyer illusion images. Spanish J Psychol 10: 3−19.
Silva MF, Brascamp JW, Ferreira S, Castelo-Branco M, Dumoulin SO, Harvey BM (2018) Radial asymmetries in population receptive field size and cortical magnification factor in early visual cortex. NeuroImage 167: 41–52.
Spiegel HG (1937) On the influence of the intermediate field on visually assessed distances (in German). Psychologische Forschung 21: 327–383.
Strasburger H, Malania M (2013) Source confusion is a major cause of crowding. J Vision 13: 24.
Strasburger H, Rentschler I, Jüttner M (2011) Peripheral vision and pattern recognition: A review. J Vision 11: 13.
Surkys T (2007) Influence of colour and luminance contrast on perceptual distortions of stimulus geometry [Ph.D. Thesis]. Kaunas University of Medicine, Kaunas, LT.
Surkys T, Bertulis A, Bulatov A (2006) Delboeuf illusion study. Medicina (Kaunas) 42: 673–681.
Tannazzo T, Kurylo DD, Bukhari F (2014) Perceptual grouping across eccentricity. Vis Res 103: 101−108.
Taouali W, Goffart L, Alexandre F, Rougier NP (2015) A parsimonious computational model of visual target position encoding in the superior colliculus. Biol Cybern 109: 549–559.
Taylor MM (1962) Geometry of a visual illusion. J Opt Soc Am 52: 565–569.
Vokoun CR, Huang X, Jackson MB, Basso MA (2014) Response normalization in the superficial layers of the superior colliculus as a possible mechanism for saccadic averaging. J Neurosci 34: 7976–7987.
Wackermann J (2017) The Oppel-Kundt illusion. In: Shapiro A, Todorović D (Eds.), Oxford compendium of visual illusion, Oxford University Press, New York, pp 303–307.
Wackermann J (2012) Determinants of filled/empty optical illusion: Influence of luminance contrast and polarity. Acta Neurobiol Exp 72: 412–420.
Wackermann J, Kastner K (2009) Paradoxical form of filled/empty optical illusion. Acta Neurobiol Exp 69: 560–563.

Wackermann J, Kastner K (2010) Determinants of filled/empty optical illusion: search for the locus of maximal effect. Acta Neurobiol Exp 70: 423–434.
Wallis TSA, Bex PJ (2012) Image correlates of crowding in natural scenes. J Vision 12: 6.
Watt RJ (1990) The primal sketch in human vision. In: Blake A, Troscianko T (Eds.), AI and the Eye, Wiley and Sons, New York, pp147-180.
Welbourne LE, Morland AB, Wade AR (2018) Population receptive field (pRF) measurements of chromatic responses in human visual cortex using fMRI. NeuroImage 167: 84–94.
Whitney D, Levi DM (2011) Visual crowding: a fundamental limit on conscious perception and object recognition. Trends Cogn Sci 15: 160–168.